Materials Research Bulletin 110 (2019) 169–173

Contents lists available at ScienceDirect

Materials Research Bulletin

journal homepage: www.elsevier.com/locate/matresbu

Synthesis of $CaWO_4$-biochar nanocomposites for organic dye removal

Ying Zhang[a], Ruimei Fan[b], Qinku Zhang[a], Ying Chen[a,c], Omaid Sharifi[a], Danuta Leszczynska[d], Rong Zhang[a], Qilin Dai[a,*]

[a] Department of Chemistry, Physics, and Atmospheric Sciences, Jackson State University, Jackson, MS 39217, USA
[b] Civil and Environmental Engineering Department, The University of Delaware, Newark, DE, 19716, USA
[c] School of Electrical & Electronic Engineering, Hubei University of Technology, Wuhan 430068, China
[d] Department of Civil and Environmental Engineering, Jackson State University, Jackson, MS 39217, USA

ARTICLE INFO

Keywords:
A. Oxides
A. Nanostructures
A. Composite
B. Chemical synthesis
B. Optical properties

ABSTRACT

Wastewater contaminated by organic dyes is a serious environmental concern. Absorption and photodegradation are two of the most common methods for organic dye molecule removal in wastewater. In this work, we develop a facile method to synthesize $CaWO_4$-biochar nanocomposites by co-precipitation method with calcium chloride and sodium tungstate in the presence of commercial biochar. The prepared $CaWO_4$-biochar nanocomposites combine the adsorption effect from biochar and photodecoloration of dyes from $CaWO_4$ nanoparticles. The influence of the ratio of $CaWO_4$ to biochar on the organic dyes including rhodamine (RhB) and methyl orange (MO) is studied. The improved organic dye removal capacity of the $CaWO_4$-biochar composites compared with bare biochar is obtained. The synthesis of $CaWO_4$-biochar composites developed in this work provide a facial technique to improve the biochar removal abilities, which can be used in industrial wastewater treatment to increase the organic dye removal efficiency.

1. Introduction

Organic dye molecules cause a serious environmental issue because large amount of dyes is released from various industries such as textile, leather, printing, plastic, food, pharmaceutical and cosmetics [1,2], leading to the production of industrial wastewater containing organic dyes. Efficient removal of organic dyes from wastewater is very necessary to the environment. Dye adsorption becomes one of the most widely used methods because it is simple, low cost, and high efficiency. In this area, the major research is focused on high-efficiency sorbent development [3], such as biomass [4], activated carbon [5], nanoparticles [6], clays [7] and fly ash [8].

In recent years, biochar as a new and promising candidate for wastewater treatment has drawn much attention due to its low cost, large surface area and functional surface groups [9]. Biochar is the solid product from biomass by hyrolysis at high temperature in very limited oxygen environment [10]. Biochar-based nanocomposites were prepared to improve the adsorption capability [11]. Most of the Biochar-based nanocomposites were synthesized during the preparation of biochar from biomass, where the starting materials, for example metal salts, were incorporated into biomass. Nanocomposites were produced as the biochar was synthesized during heat treatment [12,13]. However, this technique requires high temperature annealing process, and it is hard to control the distribution of nanoparticles in biochar. We developed a chemical synthesis method to prepare biochar-$NiFe_2O_4$ composites. $NiFe_2O_4$ magnetic nanoparticles with controlled size and structure were synthesized and incorporated into biochar to obtain magnetic biochar [14].

Photocatalytic degradation is another attractive method to remove organic substances from wastewater with its advantages of complete mineralization, no waste disposal problem, low cost and mild temperature and pressure needed [15–17]. TiO_2 and platinum catalyst are commonly used photocatalyst, however, they are not economic for large-scale water treatment [18,19]. Recently, some researchers have reported the photocatalysis action of $CaWO_4$ nanoparticles on organic dyes. Ghoreishi synthesized $CaWO_4$ nanoparticles by sonochemical reaction with Schiff base ligand, and reported the photocatalyst activity for degradation on methyl orange (MO) [20]. Sobbani-Nasab also reported the photocatalyst activity of $CaWO_4$ nanoparticles synthesized by ultrasonic digestion, and found MO degradation about 63% after 90 min illumination of UV light [21].

Biochar-based nanocomposites are a rising research topic, which could combine the advantages of biochar's with nanomaterials, resulting improved or combined functional activities [11]. In this work,

* Corresponding author.
E-mail address: qilin.dai@jsums.edu (Q. Dai).

https://doi.org/10.1016/j.materresbull.2018.10.031
Received 17 June 2018; Received in revised form 18 October 2018; Accepted 19 October 2018
Available online 23 October 2018
0025-5408/

we developed the facile method to prepare $CaWO_4$-biochar nanocomposites, which avoid the traditional high temperature annealing process. The removal of (rhodamine) RhB and (methyl orange) MO by the prepared $CaWO_4$-biochar nanocomposites were investigated compared with bare biochar. The nanocomposites show significant improved removal capacity due to the combination of the adsorption and photocatalysis properties of biochar and $CaWO_4$.

2. Experiment and measurement

2.1. $CaWO_4$-biochar synthesis

The $CaWO_4$ –biochar nanocomposites were synthesized by co-precipitation method with calcium chloride from Alfa Aesar and sodium tungstate from Alfa Aesar in the presence of biochar from Biochar Now. In a typical synthesis, 50 mL of 200 mM $CaCl_2$ aqueous solution was mixed with different amount of biochar (2.879 g for SA1, 5.758 g for SA2, 14.395 g for SA3 and 28.789 g for SA4) to make $CaWO_4$ to biochar weight ratio to be 1:1, 1:2, 1:5 and 1:10, respectively. The mixed solution was kept under vigorous stirring for 5 min. Then 50 mL of 200 mM Na_2WO_4 aqueous solution was added to the above solutions. NaOH solution was used to adjust pH value to 10, then kept stirring for 1 h. The powders were obtained by washing through vacuum filter and water until pH value is 7, then dried under vacuum at 50 °C.

2.2. Measurement

Powder X-ray diffraction (XRD) data were recorded by Rigaku MiniFlex 600 X-ray Diffractometer. Scanning electron microscopy (SEM) images and energy dispersive spectroscopy (EDS) spectrum were collected on Scanning Electron Microscopy (TESCAN LYRA3). UV–vis absorption spectra were measured by Agilent Cary 60 UV–vis Spectrophotometer. Zeta potential of the samples were measured by Zetasizer Nanoseries. Brunauer–Emmett–Teller (BET) surface area of the samples was obtained by TriStar II Plus.

2.3. Organic dye treatment

The photocatalytic activity of $CaWO_4$-biochar for organic dye molecules was evaluated by photodecoloration of RhB from ACROS Organics and methyl orange (MO) from ACROS Organics in water under the irradiation of ultraviolet (UV) light. The UV light is produced by UVP Blak-Ray mercury spot lamp (100 W, with 365 nm longwave UV). For RhB, 20 mL of 0.01 mM RhB aqueous solution and 0.03 g biochar and 0.06 g SA1, 0.045 g SA2, 0.0375 g SA3 or 0.033 g SA4. The catalyst concentrations for RhB removal of biochar, SA1, and SA4 are 1.5 g/L, 3.0 g/L, and 1.65 g/L respectively. Therefore, the same amount of biochar was involved in each sample. As for MO removal, 20 mL of 0.05 mM MO aqueous solution (pH value of 3) and 0.05 g biochar or $CaWO_4$-biocar nanocomposites samples were used. 0.05 g biochar contained in all the $CaWO_4$-biochar nanocomposites. The catalyst concentrations for MO removal of biochar, SA1 and SA4 are 2.5 g/L, 5 g/L, and 2.75 g/L respectively. The solution containing dye, biochar or $CaWO_4$-biochar nanocomposites was kept stirring under dark for 10 min. for adsorption–desorption equilibrium. Then the resulting solutions under stirring were irradiated under UV light for 30 min. The distance between the light source and the solution is 10 cm, and the real power inside the reactor is 16.45 MED/h (tested by Model PMA2100 Dual Input Radiometer). The obtained solution was filtered by 0.45 μm filter to perform the UV–vis absorption measurement. The concentration of dye molecules in the solution was monitored by absorbance with spectrophotometer to evaluate the removal capacity of the $CaWO_4$-biochar nanocomposites.

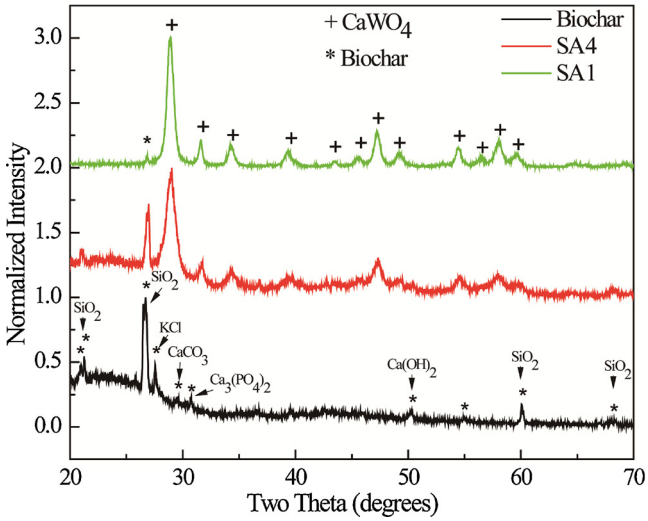

Fig. 1. XRD data of bare biochar, sample SA1 ($CaWO_4$ to biochar weight ratio = 1:1) and SA4 ($CaWO_4$ to biochar weight ratio = 1:10).

3. Result and discussion

3.1. Structure characterization

The biochar used in this work was produced with beetle killed pine as the feedstock, by slow-pyrolysis technology, and processed for up to 8 h between 550 and 600 °C according to the information from Biochar Now. SEM are used to evaluate the biochar's structure and morphology. Fig. S1 shows porous structure with long pores in diameter of 10–20 μm, leading to large surface area, which is a very typical structure for biochar. Fig. 1 shows the XRD data of bare biochar, sample SA1 and SA4. The XRD diffraction pattern of biochar shows some a broad peak at 20°–32° and some sharp peaks. The broad peak is originated from the crystal plane index of carbon (002) due to the parallel and azimuthal orientation of aromatic, partially carbonized lamellae [22]. The narrow peaks in XRD pattern is attributed to mineral phases and quartz [23]. The strong peak at 27° and weak peaks at 60° and 68° are attributed to the quartz structure SiO_2 (JCPDS no. 46-1045) [23,24]. The weak peak at 29° is from calcite $CaCO_3$ [23,24]. Weak peak at 31° is ascribed to phosphate $Ca_3(PO_4)_2$ [23,24], and the peak at 28° is caused by KCl [24]. As shown by these three XRD patterns, the relative intensity of peaks of biochar decreases with the increasing $CaWO_4$ to biochar ratio. The XRD patterns of SA1 and SA4 show both $CaWO_4$ and biochar peaks. Sample SA1 shows strong peaks from $CaWO_4$ (JCPDS no. 07-0210), and a weak peak at 27° from SiO_2 in biochar, indicating the relative large ratio of $CaWO_4$ to biochar. Sample SA4 shows the strong peak at 27° and $CaWO_4$ diffraction peaks. Compared to the ratios of diffraction peaks from biochar and $CaWO_4$ of SA1 and SA4, more $CaWO_4$ are contained in SA1, which is consistent with the starting ratios. The XRD data confirm the composite structure of $CaWO_4$-biochar, and with the $CaWO_4$ to biochar ratio increasing, more

$CaWO_4$ nanoparticles should be incorporated into biochar structure.

The chemical composition of biochar was tested by EDX technique. Fig. 2(a–e) shows EDX element mapping of sample SA1. It can be seen that $CaWO_4$ nanoparticles are

incorporated into biochar structure, and both biochar and $CaWO_4$ structure can be identified through the distribution of the elements. Fig. 2(d) shows the EDX spectrum of SA1, which confirms the co-existence of C, W, O and Ca elements.

Fig. 3 shows the SEM images of sample SA1, SA2, SA3 and SA4. As shown in the images, uniform spherical $CaWO_4$ nanoparticles in size of 200 nm can be observed, and $CaWO_4$ nanoparticles are attached to the surface or in the pores of biochar. To exam the interface of $CaWO_4$ and

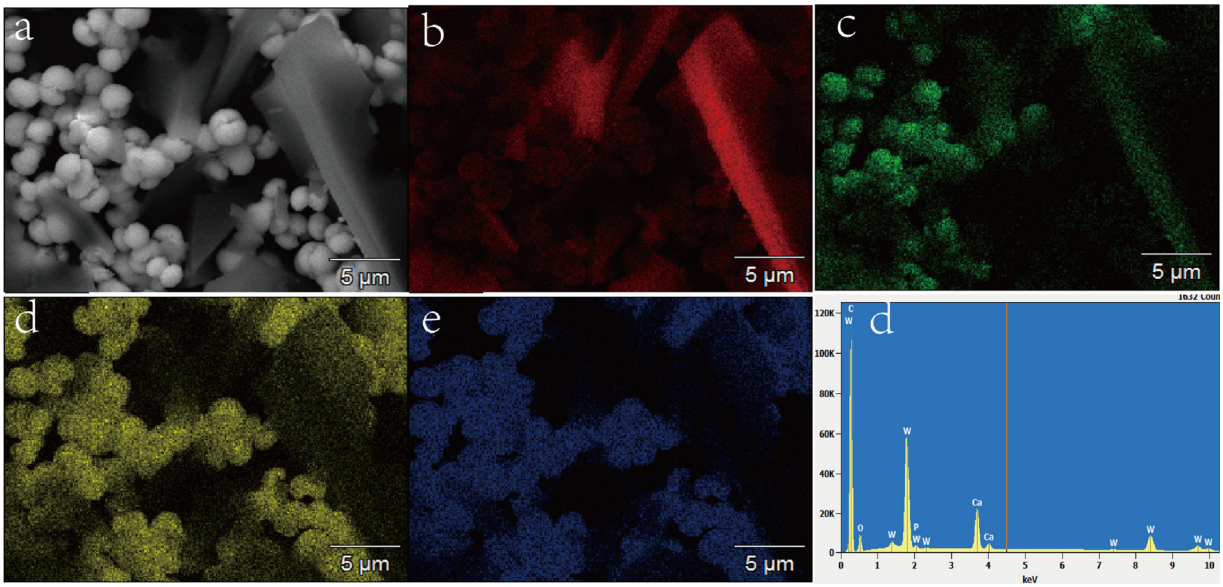

Fig. 2. EDX element mapping data of SA1. (a) Original SEM image; (b) C; (c) O; (d) Ca; (e) W; (d) EDX of SA1.

biochar, SEM image of the connection between $CaWO_4$ and biochar were measured as shown in Fig. S2. It can be observed that the attachment is relative firm, which can be identified from the stable interface between the biochar and $CaWO_4$, the stable $CaWO_4$-biochar nanocomposites formed. This can be explained by the in-situ growth of $CaWO_4$ on the surface or in the pores of biochar. With the ratio of $CaWO_4$ to biochar decreasing, less nanoparticle attached, and less surface of biochar was coated. For sample SA1, almost all the surface of biochar is coated, and the pores are stuffed with $CaWO_4$ nanoparticles, while for sample SA4, few $CaWO_4$ nanoparticles attached, and leave more surface exposed.

3.2. Organic dye removal test

The prepared $CaWO_4$-biochar nanocomposites could utilize the combination effects of absorption from biochar and photocatalytic from $CaWO_4$ nanoparticles to increase the dye removal efficiency of biochar. To test the capacity of organic dye removal, the removal of RhB and MO by prepared $CaWO_4$-biochar nanocomposite and pure biochar under irradiation of ultraviolet light were tested. To study the effects of $CaWO_4$-biochar composite on wastewater treatment compared to bare biochar, 0.01 M RhB was mixed with $CaWO_4$-biochar composites or biochar and kept stirring under UV light for 30 min. UV–vis absorption spectra were used to monitor the removal of RhB by the composites or biochar. Fig. 4(a) shows the UV–vis absorption spectra of the solution

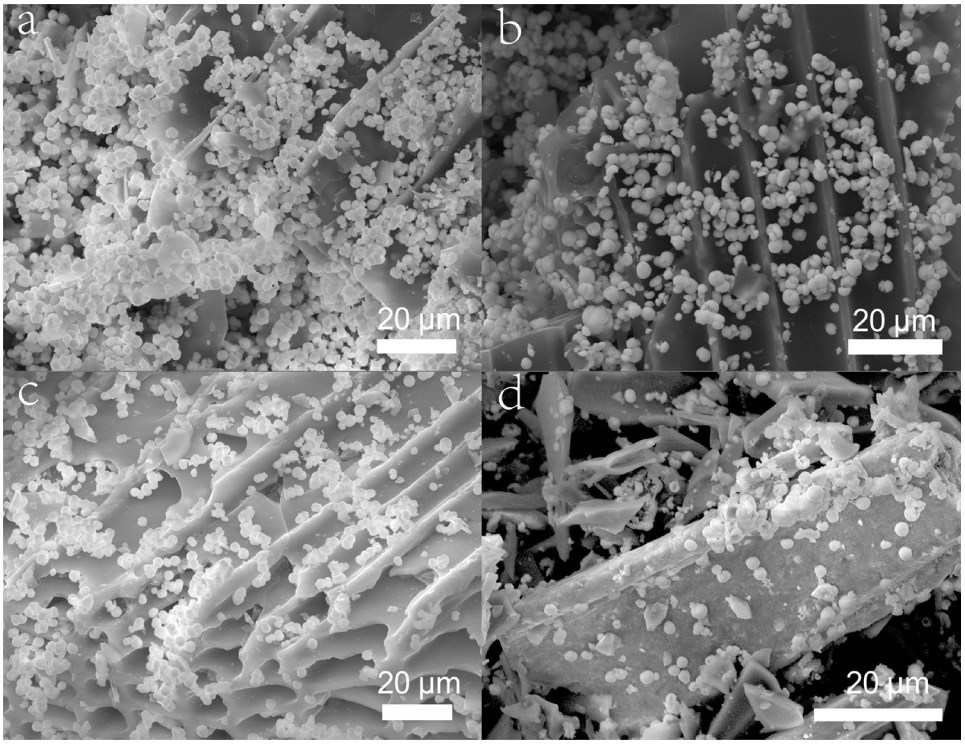

Fig. 3. SEM data of samples. (a) SA1; (b) SA2; (c) SA3; (d) SA4.

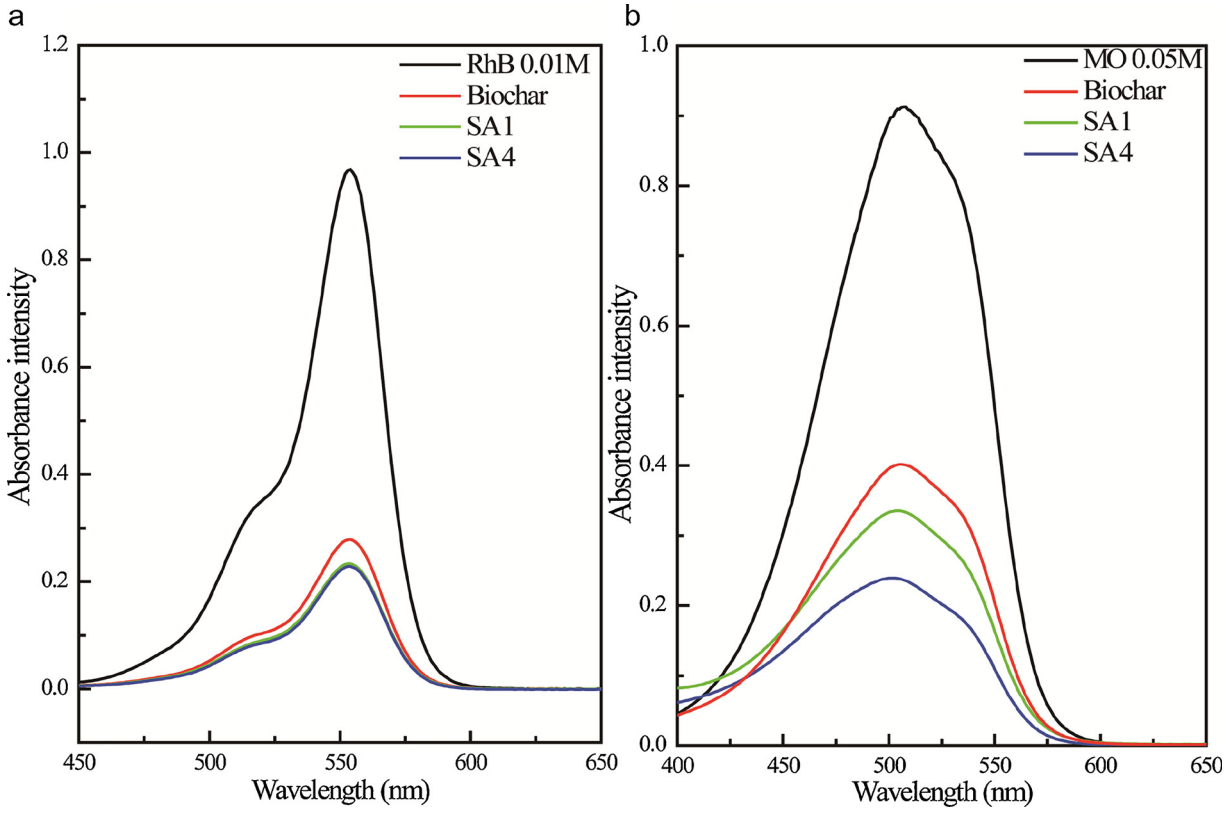

Fig. 4. The absorption spectra of solution after treatment by $CaWO_4$-biochar composites (SA1 and SA4) and biochar. (a) RhB; (b) MO.

after treatment by $CaWO_4$-biochar composites (SA1 and SA4) and biochar. In comparison, the absorption spectrum of 0.01 M RhB aqueous solution without any treatment is also presented in Fig. 4(a). Dye adsorption by biochar is the only activity for dye removal for bare biochar treatment, and 71% of RhB has been removed. Sample SA1 and SA4 show the effects of absorption from the biochar and photodecoloration from $CaWO_4$, resulting in 76% of RhB removed. With the photodecoloration from catalysis of $CaWO_4$, the removal ability has been improved by 5%. RhB solution exhibits a little lower absorbance after treated by SA4 compared to than that of SA1, indicating SA4 have a little more dye removal capacity than SA1. Fig. 4(b) shows the absorbance of MO solution after treatment with pure biochar, sample SA4 and SA1. 56% of MO has been removed by adsorption as bare biochar is used to remove MO. As for MO solution treated by sample SA1, 63% of MO has been removed. The removal capacity increases by 7%. 73% of MO has been removed as sample SA4 is used for the experiment, leading to the removal ability increased by 17%. MO photodecoloration test was performed under pH value to 3. Shan et al. studied the pH value influence on MO photodecoloration efficiency, and pointed that photodecoloration efficacy rose with the decreasing pH value. They believed that, with the anionic configuration, pH value affects surface charge of photocatalyst, and then the absorption behavior of MO on the catalyst [25]. Xu et al. pointed that the adsorption of organic dyes by biochar involved electrostatic attraction, and specific interaction between the dye molecules and the groups of $-COO^-$ and phenolic $-OH$, and surface precipitation of biochar [26]. The adsorption capacity is strongly limited by the biochar structure itself. Our results show that the dye removal of biochar has been increased by the $CaWO_4$-biochar composites for both RhB and MO. This improvement is attributed to the photodecoloration of $CaWO_4$ nanoparticles. The photo catalysis action could be ascribed with redox action introduced by light energy [20,21]. The UV light irradiation on $CaWO_4$ will induce electron–hole pairs, and then subsequently generate the hydroxyl [20,21,25], leading to removal of dyes. The photocatalytic mechanism of $CaWO_4$ on MO has been proposed by other researchers [20,21,25]. The UV light is absorbed by the $CaWO_4$ to generate electrons and holes as the light is irradiated on the $CaWO_4$ (Eq. 1). Then the photogenerated holes will react with H_2O to produce hydroxyl radicals ($OH^{\bullet}$) and H^+ [20,21,25] (Eq. 2). Hydroxyl radicals play a role as strong oxidizing agent to oxidize the dyes [20,21,25]. The photogenerated electrons will interact with O_2 to produce $O_2^{\bullet -}$ and H_2O. (Eq. 3) $O_2^{\bullet -}$ is another oxidizing specie to result in degradation of dyes. Therefore, dye degradation is an overall effect of the two species including $OH^{\bullet}$ and $O_2^{\bullet -}$ to oxidize the dyes [20,21,25].

$$CaWO_4 + UV \rightarrow CaWO_4^{\bullet} + e^- + h^+ \quad (1)$$

$$H_2O + h^+ \rightarrow OH^{\bullet} \quad (2)$$

$$e^- + O_2 \rightarrow O_2^{\bullet -} \quad (3)$$

Compared to Fig. 4(a) and (b), it can be seen that SA4 shows much better removal capacity of MO compared to that of SA1, which can be explained by the more $CaWO_4$ in SA1 may block the UV light irradiation leading to worse removal. As for the removal of RhB in Fig. 4(a), the removal capacity of SA4 is only a little better than that of SA1. This is probably due to the limited photodecoloration effect of RhB by $CaWO_4$ compared to MO. This result is consistent with the literature report [27]. 0.01 M RhB was mixed with 0.03 g $CaWO_4$ and kept stirring under UV light for 30 min to study the effect of $CaWO_4$ in the dye removal process. Fig. S3 shows the UV–vis absorption spectra of the untreated RhB and RhB treated with $CaWO_4$. It can be seen that the absorbance of RhB decreased from 0.95 to 0.93 as the solution was treated by $CaWO_4$. This indicates that very limited photocatalysis effects happened due to the limited contact during the stirring of $CaWO_4$ and RhB solution. SA1 shows about 5% decreased of RhB absorption caused by $CaWO_4$ as $CaWO_4$-biochar composite are used for dye removal (Fig. 4). While ~2% decrease of RhB absorption due to $CaWO_4$ as $CaWO_4$-only are used for dye removal (Fig. 4). We believe that more efficient photocatalysis effect happened to the adsorbed dyes on

biochar via the composite structure compared to bare $CaWO_4$ mixed with RhB solution. Biochar can play a role as a platform to allow $CaWO_4$ to interacts with dye by sufficient contact of $CaWO_4$ and dye through the $CaWO_4$-biochar composite leading to more efficient photocatalysis. Photocatalysis experiments of MO by S1 were also performed in the dark under the same conditions to confirm the photodecoloration of MO. Fig. S4 shows the photodecoloration of MO treated with S1 in the dark and UV light irradiation, and other experimental conditions are kept the same. Much more photodecoloration effect can be observed as UV light irradiation is applied to the solution compared to that of dark condition, indicating the photodecoloration of MO. The chemical function groups such as carboxyl and phenolic on biochar surface can determine biochar acidity in the aqueous solution. As shown in Fig. S5 a, lower ionic strength of 1×10^{-2} M NaCl can increase zeta potential of biochar compared to that of 1×10^{-1} M NaCl. The zeta point charge of biochar is close to 2.3, which indicates that there are numerous negative charge existing on the biochar surface. From the Fig. S5b, the zeta potential of biochar-CaWO4 is furtherly reduced compared to that of bare biochar, in other word, the incorporation of $CaWO_4$ into biochar can furtherly reduce the zeta potential of biochar. Biochar has a high porous structure with a 2.64 cm^3/g pore volume as revealed by nitrogen-adsorption isotherm curve measured in Fig. S6a, and its bet surface area is 139.02 m^2/g. In contrast, the surface area of Biochar-$CaWO_4$ is relatively low as shown in Fig. S6b and its bet surface area is 41.23 m^2/g. This indicates that $CaWO_4$ leads to reduced surface area of biochar.

4. Conclusion

In this work, we developed a facile method to synthesize $CaWO_4$-biochar nanocomposites by co-precipitation method with calcium chloride and sodium tungstate in the presence of biochar. $CaWO_4$-biochar nanocomposites with different ratios of $CaWO_4$ to biochar were prepared. The organic dye removal capacity from wastewater by the synthesized $CaWO_4$-biochar nanocomposites with different ratios of $CaWO_4$ to biochar were investigate. Compared with bare biochar, the removal capacity has been improved by 5% and 17% for RhB and MO, respectively. This improvement is explained by the photodecoloration effect from $CaWO_4$ nanoparticles. The synthesis method developed in this work provides a low cost, efficient for organic dye removal strategy.

Acknowledgements

This work was supported by National Science Foundation [Award # 1632899 and # 1332444]. Ying Chen thanks the support from National Natural Science Foundation of China21701041.

Appendix A. Supplementary data

Supplementary data associated with this article can be found, in the online version, at https://doi.org/10.1016/j.materresbull.2018.10.031.

References

[1] C. Wang, C. Feng, Y. Gao, X. Ma, Q. Wu, Z. Wang, Chem. Eng. J. 173 (2011) 92–97.
[2] V. Ganesan, C. Louis, S.P. Damodaran, Graphene oxide-wrapped magnetite nanoclusters: a recyclable functional hybrid for fast and highly efficient removal of organic dyes from wastewater, J. Environ. Chem. Eng. 6 (April (2)) (2018) 2176–2190.
[3] G. Crini, Bioresour. Technol. 97 (2006) 1061–1085.
[4] J.P. Cazon, E. Donati, Biosorption of dyes by brown algae, Strategies for Bioremediation of Organic and Inorganic Pollutants, (2018) ISBN 9781351857383.
[5] D. Desmawita, E. Yenie, S. Daud, Application of activated carbon compost raw material as adsorbent for removal of peat water dyes, J. Online Mahasiswa Fakultas Teknik 5 (April) (2018) 1–4.
[6] J.-L. Gong, B. Wang, G.-M. Zeng, C.-P. Yang, C.-G. Niu, Q.-Y. Niu, W.-J. Zhou, Y. Liang, J. Hazard. Mater. 164 (2009) 1517–1522.
[7] A. Kausar, M. Iqbal, A. Javed, K. Aftab, H.N. Bhatti, S. Nouren, J. Mol. Liq. 256 (2018) 395–407.
[8] M. EL Alouani, S. Alehyen, M. EL Achouri, M. Taibi, Potential use of moroccan fly ash as low cost adsorbent for the removal of two anionic dyes (indigo carmine and acid orange), J. Mater. Environ. Sci. 9 (2017) 3397–3409.
[9] Y. Chun, G. Sheng, C.T. Chiou, B. Xing, Environ. Sci. Technol. 38 (2004) 4649–4655.
[10] J. Lehmann, S. Joseph, Biochar for Environmental Management: Science, Technology and Implementation, Routledge, 2015.
[11] X.-F. Tan, Y.-G. Liu, Y.-L. Gu, Y. Xu, G.-M. Zeng, X.-J. Hu, S.-B. Liu, X. Wang, S.-M. Liu, J. Li, Bioresour. Technol. 212 (2016) 318–333.
[12] M. Shahadat, T.T. Teng, M. Rafatullah, M. Arshad, Colloids Surf. B Biointerfaces 126 (2015) 121–137.
[13] M. Zhang, B. Gao, S. Varnoosfaderani, A. Hebard, Y. Yao, M. Inyang, Bioresour. Technol. 130 (2013) 457–462.
[14] Y. Zhang, G. Rimal, J. Tang, Q. Dai, Mater. Res. Express 5 (2018) 025023.
[15] D.S. Bhatkhande, V.G. Pangarkar, A.A. Beenackers, J. Chem. Technol. Biotechnol. 77 (2002) 102–116.
[16] M. Chen, C. Bao, T. Cun, Q. Huang, Mater. Res. Bull. 95 (2017) 459–467.
[17] F. Chen, S. Li, Q. Chen, X. Zheng, P. Liu, S. Fang, Mater. Res. Bull. 105 (2018) 334–341.
[18] N. Daneshvar, D. Salari, A.R. Khataee, J. Photochem. Photobiol. A: Chem. 162 (2004) 317–322.
[19] K. Bubacz, B. Tryba, A.W. Morawski, Mater. Res. Bull. 47 (2012) 3697–3703.
[20] S.M. Ghoreishi, J. Mater. Sci. Mater. Electron. 28 (2017) 14833–14838.
[21] A. Sobhani-Nasab, M. Sadeghi, J. Mater. Sci. Mater. Electron. 27 (2016) 7933–7938.
[22] D. Mohan, K. Abhishek, A. Sarswat, M. Patel, P. Singh, C.U. Pittman, RSC Adv. 8 (2018) 508–520.
[23] W.-Q. Zuo, C. Chen, H.-J. Cui, M.-L. Fu, RSC Adv. 7 (2017) 16238–16243.
[24] X. Xu, X. Cao, L. Zhao, H. Zhou, Q. Luo, RSC Adv. 4 (2014) 44930–44937.
[25] Z. Shan, Y. Wang, H. Ding, F. Huang, J. Mol. Catal. A Chem. 302 (2009) 54–58.
[26] R.-k. Xu, S.-c. Xiao, J.-h. Yuan, A.-z. Zhao, Bioresour. Technol. 102 (2011) 10293–10298.
[27] Z. Zhang, W. Wang, D. Jiang, J. Xu, Appl. Surf. Sci. 292 (2014) 948–953.